Negative-chirality order in the $S = \frac{1}{2}$ kagome antiferromagnet $CdCu_3(OH)_6(NO_3)_2 \cdot H_2O$

Yoshihiko Ihara [1,*], Ryoga Hiyoshi,[1] Masakazu Shimohashi,[1] Kaoru Hayashi,[1] Ryutaro Okuma [2,3,†]
Fabio Orlandi [4], Pascal Manuel,[4] Gøran J. Nilsen,[4] and Zenji Hiroi[3]

[1]*Department of Physics, Faculty of Science, Hokkaido University, Sapporo 060-0810, Japan*
[2]*Clarendon Laboratory, University of Oxford, Oxford OX1 3PU, United Kingdom*
[3]*Institute for Solid State Physics, University of Tokyo, Kashiwa, Chiba 277-8581, Japan*
[4]*ISIS Neutron and Muon Source, Science and Technology Facilities Council, Didcot OX11 0QX, United Kingdom*

Neutron diffraction and nuclear magnetic resonance (NMR) measurements have been used to analyze the magnetic structure in the $S = \frac{1}{2}$ kagome antiferromagnet $CdCu_3(OH)_6(NO_3)_2 \cdot H_2O$. Below the magnetic ordering temperature $T_N \simeq 4\,K$, magnetic Bragg reflections at (101) and (100) were found in the neutron diffraction pattern, which suggests a $\mathbf{q} = 0$ magnetic structure. Furthermore, the vector spin chirality for the $\mathbf{q} = 0$ structure was successfully identified from the internal field direction obtained by the ^{14}N-NMR measurement, previous magnetization measurements, and magnetic symmetry analysis. Our findings point to a chirality-ordered magnetic structure with negative vector chirality and $\langle 100 \rangle$ anisotropy.

I. INTRODUCTION

The emergence of quantum magnetism on a two-dimensional (2D) kagome network has attracted considerable interest. Since a triangular unit of localized magnetic moments shares a corner with its neighbors, kagome antiferromagnets can possess a large variety of energetically degenerate spin configurations. This, as well as enhanced magnetic fluctuations on a low-dimensional magnetic network, makes them one of the most promising candidates for the realization of quantum spin liquid. Indeed, signatures of spin liquid behavior have been observed in herbertsmithite [1,2]. In some other materials, however, the material-specific small perturbations induce long-range magnetic ordering. Experimental investigations of quantum kagome magnet ground states should be conducted from a microscopic viewpoint to make progress in the understanding of the intriguing quantum effects that appear in such materials.

In this paper, we focus on the mineral $CdCu_3(OH)_6(NO_3)_2 \cdot H_2O$ [Cd-kapellasite (CdK)], in which $S = \frac{1}{2}$ Cu^{2+} spins form a 2D kagome network [3]. The nonmagnetic Cd ions are located at the center of the kagome hexagons (Fig. 1) and provide the diagonal interaction across the hexagon J_d. With a dominant nearest neighbor and small next-nearest neighbor interactions, J_1 and J_2, the main features of the magnetism in CdK is described by the $J_1 - J_2 - J_d$ model [5–7]. Within the series of these compounds, antiferromagnetic J_1 was found only in CdK and a sister compound $CaCu_3(OH)_6Cl_2 \cdot 0.6H_2O$ [Ca-kapellasite (CaK)] [8]. Experimental studies on these compounds are

crucial, as theoretical calculations that include the effect of quantum fluctuation are difficult for the antiferromagnetic $J_1 - J_2 - J_d$ model. In fact, previous studies on CdK have highlighted the effects of substantial quantum fluctuations in thermal Hall effect [9] and high-field magnetization [10]. In small magnetic fields, a magnetic anomaly with a weak ferromagnetic character was observed at $T_N \simeq 4\,K$ from the abrupt increase in susceptibility and a broad peak in the heat capacity [3]. The temperature dependence of the thermal Hall effect observed above the magnetic ordering temperatures was interpreted in the framework of the Schwinger-boson mean field theory [9,11], which suggests a finite-temperature spin liquid state with Dzyaloshinskii-Moriya (DM) interactions. A similar spin liquid behavior was also observed in CaK at corresponding temperature range from the thermal Hall effect and ^{2}D-nuclear magnetic resonance (NMR) measurements [12,13]. Magnetization studies in pulsed high magnetic fields revealed a series of field-induced valence-bond crystals at multiple magnetization plateaus [10]. Despite the exotic nature of the quantum magnetism in CdK, the magnetic structure in the ground state at small magnetic fields has not been solved. Thus far, a $\mathbf{q} = 0$ magnetic structure has been suggested from the weak ferromagnetic behavior in magnetization [3]. However, even limiting the search to $\mathbf{q} = 0$ structures, various types of spin configurations can be constructed, although authors of theoretical studies suggest that the thermal Hall conductivity would vanish for some of these [14]. Microscopic measurements should therefore be performed to determine the actual magnetic structure.

The magnetic structures possible for the $J_1 - J_2 - J_d$ model in the nearest neighbor limit are based on the 120° spin configuration, for which the neighboring two spins always form a relative angle of 120°. Classical calculations [15] suggest that $\mathbf{q} = 0$ or $\sqrt{3} \times \sqrt{3}$ structures are favored as ground states in a large parameter space. Noncoplanar cuboc structure

*yihara@phys.sci.hokudai.ac.jp
†ryutaro.okuma@physics.ox.ac.uk

is also proposed in a restricted area around $J_d = 0$. In the case of CaK, the negative chirality $\mathbf{q} = 0$ structure is stabilized by the energy gain of DM interaction [12,16,17], which underlines the relevance of the latter interaction in establishing a theoretical model for the kagome antiferromagnets.

The magnetic interactions in CdK were estimated from bulk susceptibility as $(J_1/\mathrm{K}, J_2/J_1, J_d/J_1) = (45.4, 0.1, 0.18)$ [10]. The energy scale of DM interaction was suggested as ~ 4 K, which is comparable with the long-range ordering temperature. According to the classical theory, these parameter sets suggest a $\mathbf{q} = 0$ structure as the ground state. However, in the case of a $\mathbf{q} = 0$ structure, two distinct spin configurations are possible with the same translation vector. Namely, the vector chirality of three spins on one triangle can be either negative [negative vector chirality (NVC)] or positive [positive vector chirality (PVC)]. These various spin configurations are difficult to distinguish using neutron diffraction measurements, especially when the sample mass is limited, and the ordered moments are reduced by the quantum fluctuations.

NMR measurement is an excellent tool to determine the local spin configuration. By examining the internal fields at the target nuclei from the NMR spectra, the spin configurations around the sites can be identified. The sign of the vector chirality in a $\mathbf{q} = 0$ structure can be distinguished using the orientation of dipole fields at the threefold axis of a triangle. The internal-field direction is an important indicator of the spin configuration, as it eliminates the requirement for quantitative estimate of the field strength, which is frequently influenced by many parameters. While sensitive to the local spin configuration, NMR measurements are incapable of determining the global translation vector. Therefore, we performed ^{14}N-NMR measurement for CdK together with neutron diffraction measurements. The complementary combination of neutron diffraction and NMR study allowed us to identify the ground state magnetic structure.

II. EXPERIMENTAL

Single crystals of CdK used for the NMR experiment were grown by the hydrothermal transport method [3]. The NMR spectra were measured in the magnetic fields **H** applied along the [001] and [120] directions. For the sharp lines in **H** ∥ [001], the full spectra were obtained by the fast Fourier transform (FFT) of the spin-echo signal at a fixed field. Since the spectral width becomes significantly broad due to the effect of nuclear quadrupolar interaction for **H** ∥ [120], we measured the field-sweep spectra at a fixed frequency. The FFT intensity was recorded during the field sweep. We measured the temperature dependence of NMR frequency shift at high temperatures >100 K for $H \parallel [001]$, but the peak positions hardly shift, suggesting that the transferred hyperfine interactions between the Cu^{2+} electronic spins and ^{14}N nuclear spins are compensated by the direct dipole interactions, which were calculated to be ~ 100 mT/μ_B.

The powder sample of CdK for the neutron diffraction experiment was enriched with deuterium and ^{114}Cd because of large incoherent scattering of hydrogen and strong neutron absorption of natural Cd. Details of sample preparation are presented in the Supplemental Material [18]. Magnetization measurements confirmed that the isotope-substituted powder
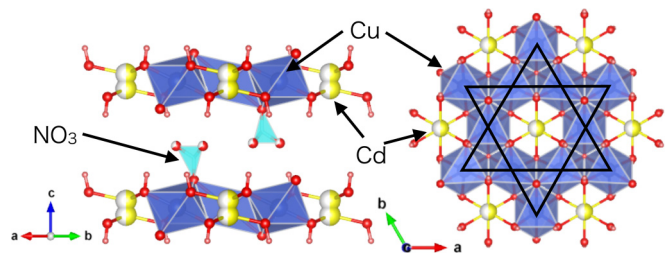

FIG. 1. The crystal structure of CdK. Blue, yellow/white, red, cyan, and salmon spheres represent copper, cadmium, oxygen, nitrogen, and hydrogen atoms, respectively. The nitrate ion coordinated to the copper ion possesses orientational disorder across three positions. The crystal structure was drawn with VESTA [4].

has the same transition temperature of 4 K as in the natural isotopic sample of CdK. Neutron diffraction experiments were performed on the time-of-flight diffractometer WISH at ISIS Neutron and Muon Source, UK [19]. Data were recorded on 10 fixed angle detector banks joined in five pairs, each bank covering $32°$ in the scattering plane, at temperatures of 1.6 and 10 K.

III. RESULTS AND DISCUSSION

A powder neutron diffraction experiment was performed to determine the nuclear and magnetic structures of CdK below and above the Néel temperature of 4 K. The observed and calculated powder diffraction patterns at 10 K are shown in Fig. 2(a). The initial structural model was based on the parameters from the single crystal study [20]. The Rietveld refinement using the FULLPROF suite [21] converged with space group $P\bar{3}m1$ and successfully determined the lattice constants $a = b = 6.5261(2)$ Å, $c = 6.9989(6)$ Å, and all the positions of atoms including deuterium/hydrogen. A schematic image of the structure is shown in Fig. 1. The technical details of Rietveld refinement and a list of atomic positions are presented in the Supplemental Material [18].

A low-temperature pattern collected at 1.6 K showed no additional peaks, suggesting either absence of incommensurate structures or the $\sqrt{3} \times \sqrt{3}$ cuboc/octahedral order with propagation vector of $\mathbf{q} = (\frac{1}{3}, \frac{1}{3}, 0)$ or $(\frac{1}{2}, 0, 0)$ or an ordered moment below the detection limit of the instrument. As shown in Fig. 2(b), subtraction of the dataset at 1.6 K from the one at 10 K revealed magnetic intensity on the (101) reflection for the data collected at average 2θ of $54°$ and on the (100) reflection for the data collected at average 2θ of $54°$ and $27°$.

This points to the presence of a $\mathbf{q} = 0$ magnetic order in CdK. A $\mathbf{q} = 0$ antiferromagnetic order in the classical Heisenberg model on the kagome lattice is characterized by either positive or negative signs of the vector chirality in each triangle. Figure 2(c) illustrates four candidate magnetic structures, PVC$_1$, PVC$_2$, NVC$_1$, and NVC$_2$, which are represented as ψ_1, ψ_2, $2\psi_4 + \psi_5$, and $2\psi_7 + \psi_9$ using the basis vectors of $P\bar{3}m1$ with the $\mathbf{q} = 0$ propagation vector as described in Ref. [3]. These $\mathbf{q} = 0$ states are favored by DM interaction and local bond-dependent anisotropy [3]. Comparison of the observed and calculated diffraction patterns is shown in Fig. 2(d). We note that the NVC$_1$ and NVC$_2$ structures produce an identical diffraction pattern. The PVC$_2$ structure
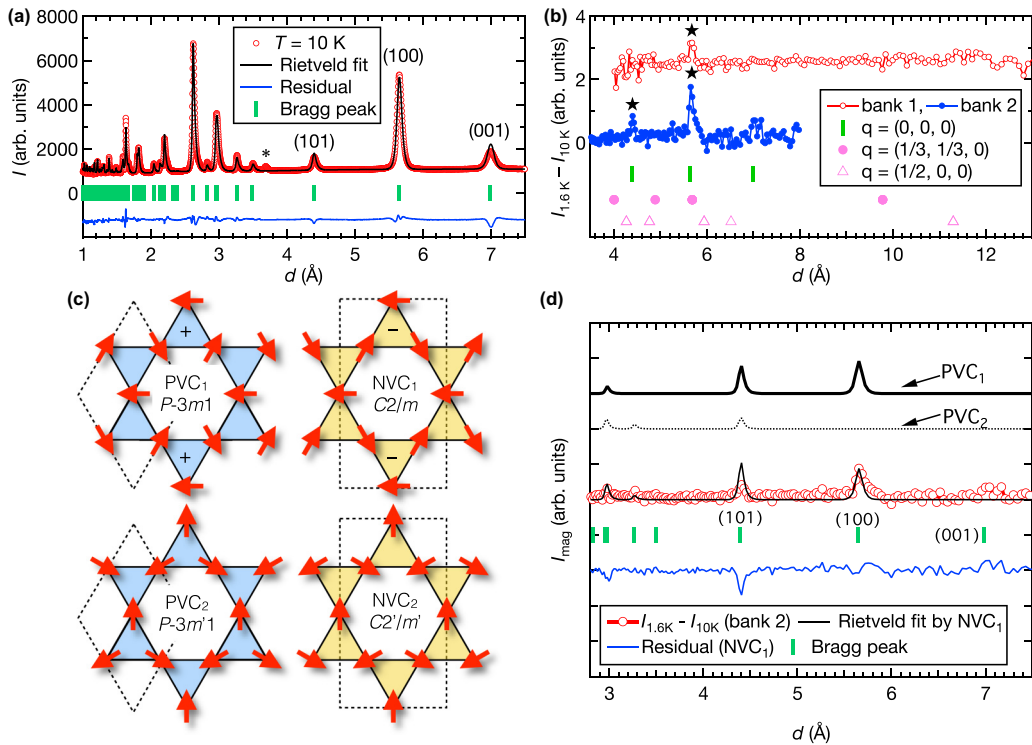
FIG. 2. Neutron diffraction results of CdK. (a) The nuclear Rietveld refinement of the neutron diffraction pattern at 10 K. The red open circles, black line, and blue line indicate the observed, calculated, and residual patterns, respectively. The green bars represent the positions of the nuclear Bragg peaks. Impurity contributions shown by asterisks are excluded from the refinement. (b) The subtracted diffraction pattern of the dataset at 1.6 K from the one at 10 K of the detector with average 2θ of $27°$ (red line with open circles) and $54°$ (blue line with filled circles), respectively, collected on the WISH diffractometer. The observed magnetic Bragg peaks are shown by black stars. The green bar, pink filled circle, and open triangle represent the expected positions of Bragg peaks corresponding to $\mathbf{q} = (0, 0, 0)$, $(\frac{1}{3}, \frac{1}{3}, 0)$, and $(\frac{1}{2}, 0, 0)$. (c) Candidate antiferromagnetic structures with a propagation vector of $\mathbf{q} = (0, 0, 0)$ in the kagome lattice. PVC_1 (PVC_2) and NVC_1 (NVC_2) structures are the ordering of positive and negative vector chirality in the presence of $\langle 100 \rangle$ ($\langle 120 \rangle$) anisotropy, respectively. The magnetic unit cell is shown by the dotted lines. In the $C2/m$ and $C2'/m'$ structures, the setting of the magnetic unit cell is changed to $(a', b', c') = (2a + b, b, c)$ from the parent $P\bar{3}m1$ structure. (d) Magnetic Rietveld refinement. Red open circles with the thin black line, blue line, and green bars represent the observed magnetic diffraction pattern, the calculated pattern of the NVC_1 structure, the residual of the fitting by the NVC_1 structure, and the position of the Bragg peaks, respectively. The thick and dotted black lines indicate the calculated diffraction pattern of PVC_1 and PVC_2, respectively.

can be excluded because of null intensity at the (100) position in the simulated diffraction pattern. The patterns of PVC_1 and NVC_1/NVC_2 are all consistent with the observed ones, and both structures show finite intensity at (100) and (101) and no intensity at (001).

However, the experimentally observed weak ferromagnetic moment in the ab plane is forbidden by symmetry in the PVC_1 structure, while both NVC_1 and NVC_2 structures are compatible with a net moment in the ab plane [3]. The $C2/m$ symmetry of the NVC_1 structure allows a ferromagnetic moment only along the $\langle 100 \rangle$ direction of the parent $P\bar{3}m1$ structure, whereas the moment in the NVC_2 structure lies along the $\langle 210 \rangle$ direction. This symmetry information joined with the torque magnetometry measurements which indicate the $\langle 100 \rangle$ direction as the local easy axis clearly indicates the NVC_1 structure as the most likely solution. The refinement with the latter model yielded an ordered moment as small as $0.21(1)\,\mu_B$, suggesting strong fluctuations remaining in the ground state. It should be noted that we did not consider the effect of the in-plane canting observed in previous magnetization measurements due to its very small magnitude.

To further confirm the NVC_1 structure, NMR measurements were used as a complementary probe. To discriminate between the PVC and NVC structures, we used the fact that the two models yield different orientation of the dipole fields at the N sites. For the PVC configuration, the dipole fields are perpendicular to the kagome plane, and their magnitude is maximum for PVC_2 and zero for PVC_1. In the case of NVC, dipole fields with a constant magnitude appear in the kagome plane [16]. Therefore, we measured the ^{14}N-NMR spectra at low temperatures across T_N in both field directions, namely, the [120] and [001] directions.

The 2D kagome layers are separated by NO_3 ions, and the N sites are located near the center of the Cu triangle, as shown by the enlarged picture in Fig. 3(b). The positional disorder of N sites creates additional features in the NMR spectra through the electric quadrupolar interaction in fields parallel to the kagome plane. In contrast, when the field is perpendicular to the kagome plane, the positional disorder of N sites does not split the NMR spectra because these N positions are related by the threefold symmetry around the [001] direction. Figure 3(a) shows the ^{14}N-NMR spectrum at room temperature

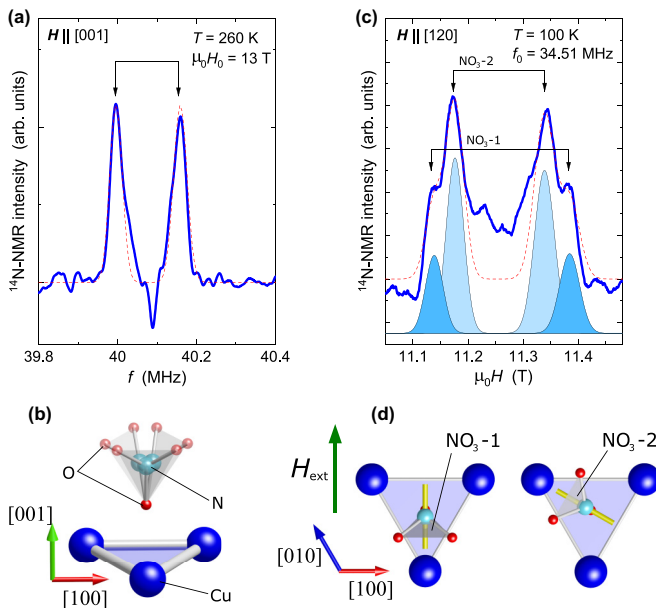FIG. 3. ^{14}N-nuclear magnetic resonance (NMR) spectra for single-crystalline CdK at high temperatures measured in (a) **H** ∥ [001] and (c) **H** ∥ [120]. Two-peak structure typical for $I = 1$ nuclear spin is observed in (a), while four peaks were observed in (c) because of the positional disorder of NO$_3$ ions. The shadowed four peaks are the result of spectrum simulation (see text for details). The sum of these four peaks is represented by the red dotted line. (b) Positional disorder of NO$_3$ ions located on a Cu triangle. Three possible NO$_3$ sites are randomly occupied. (d) In-plane structure of NO$_3$ ions. The orientation of the main principal axis of the electric field gradient (EFG) is indicated by a bar on the N sites. When the external field H_{ext} is applied along the [120] direction, N sites at NO$_3$-1 and NO$_3$-2 show different quadrupolar splitting.

FIG. 4. Temperature dependence of ^{14}N-nuclear magnetic resonance (NMR) spectra in (a) **H** ∥ [001] and (b) **H** ∥ [120]. The dotted green lines are the results of multipeak Gaussian fits. (c) Temperature dependence of $1/T_1$ in $\mu_0 H \simeq 11$ T. A peak in $1/T_1$ at $T_N = 3$ K confirms a magnetic transition at ∼11 T, even though no apparent change was observed in the spectral shape.

in the fields parallel to the [001] direction. As the nuclear spin of ^{14}N is $I = 1$, two peaks from $m = 1 \leftrightarrow 0$ and $m = 0 \leftrightarrow -1$ transitions were observed. Downward spike noise at 40.1 MHz originates from a small offset in the spin-echo signal.

From the separation of these two peaks, the NQR frequency along the [001] direction is estimated as 164 kHz. The lattice symmetry imposes that one of the principal axes of the electric field gradient (EFG) is perpendicular to the mirror plane that includes the target N sites. The other two axes are in the mirror plane. As the three covalent N-O bonds dominantly contribute to the EFG, the principal axis that has the largest EFG should be perpendicular to the O triangle of NO$_3$ unit, as shown in Fig. 3(d). The randomly occupied three N sites generate three different orientations of EFG principal axes in the *ab* plane. Thus, for the in-plane fields, the orientational disorder of the NO$_3$ units introduces an additional feature in the ^{14}N-NMR spectrum. Figure 3(c) shows the ^{14}N-NMR spectrum for **H** ∥ [120], in which we found two sets of two peaks. The peaks with larger splitting originate from the N sites with the EFG principal axis parallel to the external fields [NO$_3 - 1$ in Fig. 3(d)], while those with narrower splitting are from NO$_3$ at the other two positions (NO$_3$-2). We estimated the NQR frequency along the main [120] direction from the peak separation for the NO$_3$-1 site as 790 kHz. The splitting
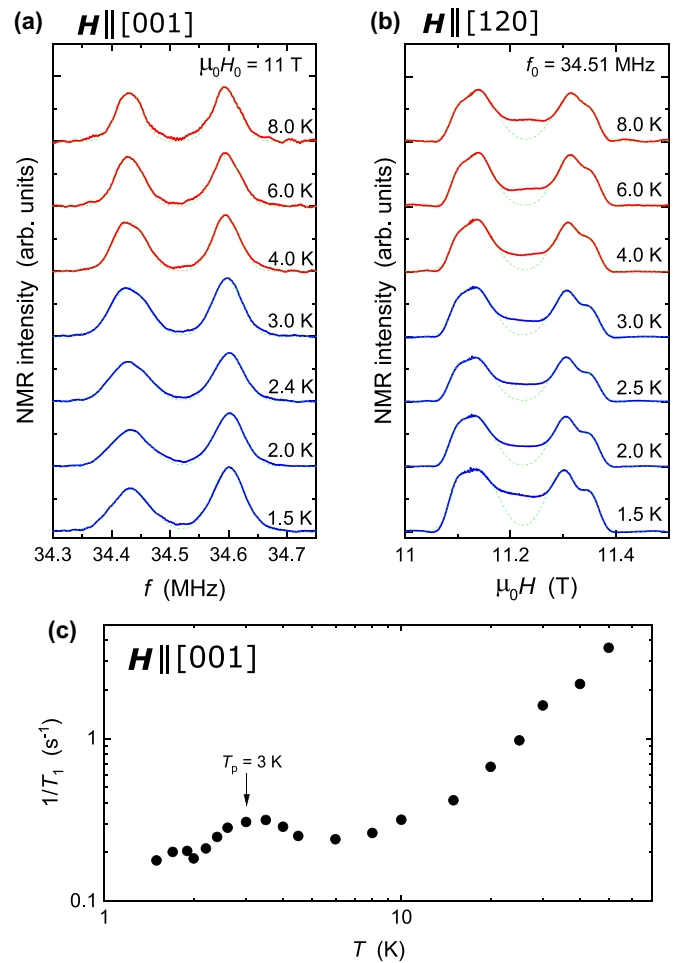
for NO$_3$-2 sites is then calculated as 0.145 T [18], which is in perfect agreement with the experimentally obtained peak separation of 0.16 T. The peak intensity of NO$_3$-2 sites is larger than that for NO$_3$-1 sites because there are twice as many sites. We simulated the ^{14}N-NMR spectrum for **H** ∥ [120] using the parameters obtained above. The result is shown in Fig. 3(c) as the shadowed peaks and dotted line. The discrepancy around the center of four peaks comes from the imperfect orientational order of the NO$_3$ units.

Knowing the above peak assignments, we measured the temperature variation of ^{14}N-NMR spectra on crossing T_N. Figures 4(a) and 4(b) show the NMR spectra for both field directions <8 K. Although only a small modification of the spectral shape was observed around T_N, we confirmed the magnetic transition temperature at ∼11 T by $1/T_1$ measurements in **H** ∥ [001]. As shown in Fig. 4(c), a peak in $1/T_1$ was observed at $T_N = 3$ K, which is associated with the critical magnetic fluctuations near the magnetic phase transition. Here, T_N in 11 T is slightly lower than that at zero fields because the antiferromagnetically ordered state is suppressed
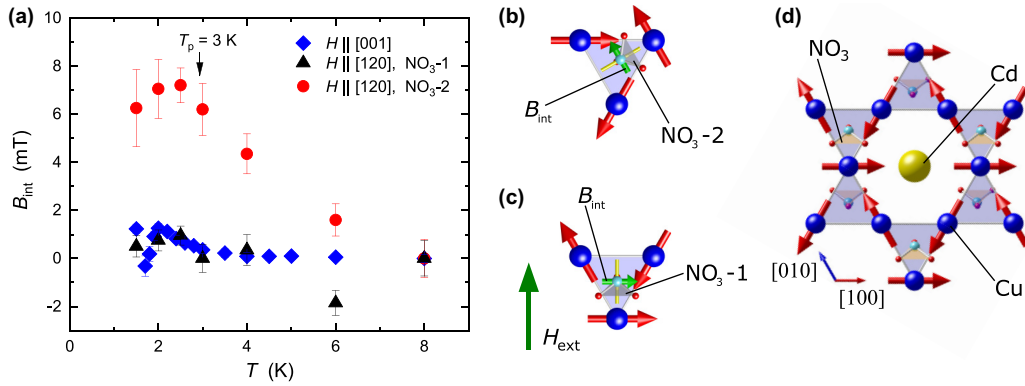
FIG. 5. (a) Internal fields obtained from the nuclear magnetic resonance (NMR) shift. Negligibly small internal fields were observed at low temperatures in $\mathbf{H} \parallel [001]$ and $\mathbf{H} \parallel [120]$ for NO_3-1 sites. (b) and (c) Negative-chirality spin configuration for Cu spins and dipole fields at the N site. The direction of internal fields is indicated by an arrow on the N site. B_{int} at the NO_3-1 site is perpendicular to H_{ext}, while the angle between B_{int} and H_{ext} is 30° at the NO_3-2 site. (d) Orientation-ordered crystal structures with anisotropy axis along [100] directions. NO_3 units are located above and below the kagome plane alternatively at each triangle and are reproduced by the inversion symmetry within a unit cell. Magnetic structures for both orientations are represented by red arrows on the Cu sites. Among three spins on one triangle, one spin is always parallel to the anisotropy axis.

by the magnetic fields. Across the magnetic phase transition at T_N, no change in spectral shape was observed for $\mathbf{H} \parallel [001]$. The spectra in $\mathbf{H} \parallel [120]$ show a shift in the peak position only for the NO_3-2 sites, which results in an asymmetric spectral shape at the lowest temperature.

The temperature dependence of the ^{14}N-NMR shift is determined by fitting the NMR spectra with multipeak Gaussians, and the results for three independent ^{14}N sites are shown in Fig. 5(a). The internal fields along the external field directions are estimated by taking the average peak positions for the quadrupolar-split peaks, and the internal fields in the ordered state are defined as $\Delta B_{int}(T) = B_{int}(T) - B_{int}(8\,\mathrm{K})$. A significant temperature dependence is observed only for the NO_3-2 sites in $\mathbf{H} \parallel [120]$, which leads us to conclude a local spin arrangement consistent with the negative chirality $\mathbf{q} = 0$ structure.

In the $\mathbf{q} = 0$ state with 120° spin configuration, the hyperfine fields from the ordered moments are canceled at the N sites. Therefore, we assume the direct dipole fields as the origin of the NMR shift in the ordered state. The PVC spin configuration is excluded from the absence of internal fields along the c direction in the experimental data explained above. We also find that, even in $\mathbf{H} \parallel [120]$, the internal fields are absent at NO_3-1 sites. This site dependence is explained by the spin-locking in the $\mathbf{q} = 0$ structure. The direction of the internal fields depends on the global spin orientation in the NVC_1 and NVC_2 structures. When the spin direction with respect to the EFG principal axis is locked, the internal field at N site always has a fixed angle against the EFG axis, as shown in Figs. 5(b) and 5(c). In the case of the NVC_1 configuration shown in Fig. 5, the internal fields are parallel to the kagome plane and perpendicular to the EFG axis and thus have no effect on the NMR shift when the external fields are parallel to the main EFG axis, which is the case for NO_3-1 sites. A finite NMR shift by the internal fields can be observed only for NO_3-2 sites, for which the angle between the external and internal fields is 30°. On the other hand, when all spins are rotated by 90° (NVC_2), the NMR shift should be observed for the sites with fields parallel to the EFG axis, that is, the NO_3-1

sites with the largest quadrupolar splitting. As no internal fields were observed at the NO_3-1 sites, a spin-locked NVC_1 structure is strongly suggested as the ground state, in agreement with the neutron data and the symmetry considerations.

In this analysis, we did not consider the canting of moments toward the c direction because the c component of the moments estimated from the magnetization measurement is two orders of magnitude smaller than the in-plane component [3].

Now we estimate the size of the ordered moments from the internal fields in the ordered state ΔB_{int}. As the internal field projected to the external field direction is ∼7 mT at $T < T_N$, the magnitude of the dipole field is estimated as $7/\cos(30°) = 8$ mT. When the full moments of 1 μ_B form the NVC spin configuration in CdK, the dipole fields at N sites are computed as 40 mT. By comparing this estimate and experimentally obtained ΔB_{int}, the size of the ordered moment can be estimated as 0.2 μ_B. This is consistent with the value obtained from the neutron diffraction measurement.

The NVC state was reported in CaK from ^{35}Cl- and ^{2}D-NMR studies [12,16]. In CaK, however, the spin directions are not locked to the crystal axes. The resulting NMR spectra in the ordered state show a broadening rather than a uniform shift. By contrast, the negligibly small spectral broadening in CdK clearly suggests the spin-locked state. As the spin direction is always fixed with respect to the EFG principal axis, we suggest that the orientation of NO_3 is responsible for the spin locking. Small modification of Cu-O-Cu bonding through O of the NO_3 units would introduce bond-dependent exchange matrices, which in turn produce a magnetic anisotropy with respect to the ⟨100⟩ direction.

An example of the distorted structure obtained by ISODISTORT [18,22,23] is illustrated in Fig. 5(d). The structure belongs to $C2/m$, which is a subgroup of the original $P\bar{3}m1$ and has no disorder of the NO_3 units. The sixfold rotational symmetry of the in-plane magnetization torque data [3] suggests that this $C2/m$ structure should coexist with the other two domains related by threefold rotation with equal probability. While the limited crystallinity of the powder sample

prevents us from elucidating the long-range order of NO_3 by neutron scattering [18], we suggest that the orientation of NO_3 should be ordered at high temperatures because the disorder of NO_3 orientation within a short distance would create a distribution in the internal field at the N site, which contradicts the uniform internal field evidenced from the shift in ^{14}N-NMR spectra without broadening [Fig. 4(b)].

It is worth underlining here that, even if the nuclear symmetry above T_N is reduced to $C2/m$, the symmetry considerations described in the neutron diffraction analysis still stand since $C2/m$ is an isotropy subgroup of the $P\bar{3}m1$ structure.

To summarize, we have performed neutron diffraction and ^{14}N-NMR measurements of the 2D kagome antiferromagnet CdK and identified the $\mathbf{q} = 0$ state with the chirality-ordered NVC_1 structure as the system ground state. The $\mathbf{q} = 0$ state is consistent with the classical calculation with the $J_1 - J_2 - J_d$ model, but in CdK, DM interactions and modified exchange interaction due to the likely orientational order of NO_3 units are also important to stabilize the spin-locked NVC_1 structure. The ordered moment is significantly reduced, even at the lowest temperature, due to strong quantum fluctuations. Since the magnetic ground state has been determined with

high confidence, the many fascinating phenomena observed in CdK can now be understood in terms of quantum fluctuations activated on the background of weak NVC_1 order. In fact, suppression of thermal Hall conductivity toward the ordered state [9] is consistently explained by the NVC_1 structure because the magnetic symmetry prohibits the thermal Hall effects in the case of NVC_1 [14].

[1] M. P. Shores, E. A. Nytko, B. M. Bartlett, and D. G. Nocera, J. Am. Chem. Soc. **127**, 13462 (2005).

[2] M. R. Norman, Rev. Mod. Phys. **88**, 041002 (2016).

[3] R. Okuma, T. Yajima, D. Nishio-Hamane, T. Okubo, and Z. Hiroi, Phys. Rev. B **95**, 094427 (2017).

[4] K. Momma and F. Izumi, J. Appl. Crystallogr. **44**, 1272 (2011).

[5] B. Fåk, E. Kermarrec, L. Messio, B. Bernu, C. Lhuillier, F. Bert, P. Mendels, B. Koteswararao, F. Bouquet, J. Ollivier *et al.*, Phys. Rev. Lett. **109**, 037208 (2012).

[6] B. Bernu, C. Lhuillier, E. Kermarrec, F. Bert, P. Mendels, R. H. Colman, and A. S. Wills, Phys. Rev. B **87**, 155107 (2013).

[7] Y. Iqbal, H. O. Jeschke, J. Reuther, R. Valenti, I. I. Mazin, M. Greiter, and R. Thomale, Phys. Rev. B **92**, 220404(R) (2015).

[8] H. Yoshida, N. Noguchi, Y. Matsushita, Y. Ishii, Y. Ihara, M. Oda, H. Okabe, S. Yamashita, Y. Nakazawa, A. Takata *et al.*, J. Phys. Soc. Jpn. **86**, 033704 (2017).

[9] M. Akazawa, M. Shimozawa, S. Kittaka, T. Sakakibara, R. Okuma, Z. Hiroi, H.-Y. Lee, N. Kawashima, J. H. Han, and M. Yamashita, Phys. Rev. X **10**, 041059 (2020).

[10] R. Okuma, D. Nakamura, T. Okubo, A. Miyake, A. Matsuo, K. Kindo, M. Tokunaga, N. Kawashima, S. Takeyama, and Z. Hiroi, Nat. Commun. **10**, 1229 (2019).

[11] H.-Y. Lee, J. H. Han, and P. A. Lee, Phys. Rev. B **91**, 125413 (2015).

[12] Y. Ihara, K. Matsui, Y. Kohama, S. Luther, D. Opherden, J. Wosnitza, H. Kühne, and H. K. Yoshida, J. Phys. Soc. Jpn. **90**, 023703 (2021).

[13] H. Doki, M. Akazawa, H.-Y. Lee, J. H. Han, K. Sugii, M. Shimozawa, N. Kawashima, M. Oda, H. Yoshida, and M. Yamashita, Phys. Rev. Lett. **121**, 097203 (2018).

[14] A. Mook, J. Henk, and I. Mertig, Phys. Rev. B **99**, 014427 (2019).

[15] L. Messio, C. Lhuillier, and G. Misguich, Phys. Rev. B **83**, 184401 (2011).

[16] Y. Ihara, H. Yoshida, K. Arashima, M. Hirata, and T. Sasaki, Phys. Rev. Research **2**, 023269 (2020).

[17] K. Iida, H. K. Yoshida, A. Nakao, H. O. Jeschke, Y. Iqbal, K. Nakajima, S. Ohira-Kawamura, K. Munakata, Y. Inamura, N. Murai *et al.*, Phys. Rev. B **101**, 220408(R) (2020).

[18] See Supplemental Material at http://link.aps.org/supplemental/10.1103/PhysRevB.106.024401 for technical details of Rietvelt refinement and estimate of NQR splitting width.

[19] L. C. Chapon, P. Manuel, P. G. Radaelli, C. Benson, L. Perrott, S. Ansell, N. J. Rhodes, D. Raspino, D. Duxbury, E. Spill *et al.*, Neutron News, **22**, 22 (2011).

[20] H. R. Oswald, Helv. Chim. Acta. **52**, 2369 (1969).

[21] J. Rodríguez-Carvajal, Phys. B: Condens. Matter **192**, 55 (1993).

[22] H. T. Stokes, D. M. Hatch, and B. J. Campbell, ISODISTORT, ISOTROPY Software Suite, iso.byu.edu.

[23] B. J. Campbell, H. T. Stokes, D. E. Tanner, and D. M. Hatch, J. Appl. Cryst. **39**, 607 (2006).

[24] https://doi.org/10.5286/ISIS.E.95961807